

## Research Paper

# GBD-DART-II: 175 MHz Polarimetric Observation of Pulsars from Gauribidanur and a New Pulsar Signal Processing Pipeline

Arul Pandian B<sup>1,2</sup>, Joydeep Bagchi<sup>1</sup>, Prabu Thiagaraj<sup>2</sup>, K.B.Raghavendra Rao<sup>2</sup>, Vinutha Chandrashekhar<sup>2</sup>

<sup>1</sup>The Christ (Deemed to be University), Bangalore., <sup>2</sup>Raman Research Institute, Bengaluru, India.

arXiv:2602.00736v1 [astro-ph.IM] 31 Jan 2026

## Abstract

A new pulsar signal-processing pipeline has been developed for observing pulsars with the Diamond Array Radio Telescope (DART) at the Gauribidanur radio observatory (13.604 N, 77.427 E). The array consists of 32 off-axis dual-polarised LPDAs, with a nominal gain of 22 dBi between 130 and 350 MHz and a 15-degree HPBW at 175 MHz, and it performs transit observations on pulsars. Custom-developed analogue signal conditioning, transmission, and a digital backend are incorporated to record the data. A real-time data-capture and analysis tool has been developed that receives band-limited time-series data and outputs voltages from a transient buffer, as well as full-polar spectral data at both high and low resolutions, suitable for transient searches and pulsar studies. Additionally, full-polar folded profile archives are generated for known pulsars in subintegrations and both coherent and incoherent dedispersion. An all-day monitoring is implemented that continuously records a one-second averaged spectrum. Custom-developed Python routines, FFT libraries, DSPSR, PSRCHIVE, and Presto modules have been used to build the pipeline. The functionalities of the pipeline were validated with artificially generated pulsar signals and strong celestial sources before it was released for routine observations. Presently, the pipeline is configured to observe pulsars between 170 and 196 MHz, with a daily cadence. Recorded data are reduced in-line immediately following each observation, nearly matching the observation time at a 1:1 ratio. An Intel i9 server captures the data, and an AMD R9 CPU does the primary data reduction. The archives are routinely backed up to a remote system via the internet. The paper presents the architecture of the signal processing pipeline developed, its validation, and initial polarimetric results observing five bright pulsars at 175 MHz. Results also include RM estimates and single-pulse study results for B0953+08, B0531+21, and B1133+16, as well as from monitoring the spin-down of the Crab pulsar over 200 days of observation. Finally, it presents a discussion on the potential improvements for the array.

**Keywords:** Pulsar observation, Polarisation, Pulsar data processing pipelines, Rotation Measure, RF receivers, Single Pulse

(Received xx xx xxxx; revised xx xx xxxx; accepted xx xx xxxx)

## 1. Introduction

Low-frequency radio pulsar observations are crucial for understanding pulsar emission mechanisms, galactic magnetic fields from the observed Faraday rotation (Sobey C. 2017), and the interstellar medium via scattering and dispersion measurements. The recent efforts to detect low-frequency gravitational waves utilise pulsar timing arrays (PTAs) (Foster R.S. and Backer D.C. 1990), formed by a collection of millisecond pulsars (MSBs) in our galaxy. Continued observations and correlation of the pulse time-of-arrival (ToA) errors from the MSBs located at vantage positions serve to implement a galactic-scale interferometer and aid in investigating disturbances to the space-time metric due to a passing gravitational wave (Edwards R.T. *et al.* 2006). Precise knowledge of the dispersion measure (DM) is essential for accurate ToA estimation of a pulsar. The DM estimation from low-frequency observations yields accuracies an order of magnitude greater than with higher-frequency observations alone (Krishnakumar M.A. *et al.* 2021). Such observations also provide our most direct clues to the structure of the magnetic fields around pulsars. They are

essential in the case of millisecond pulsars, where radio emission necessarily originates very close to the surface of the neutron star.

The linearly polarised emission in the rotating vector model (RVM) tracks changes in the dipolar magnetic field line planes, which causes the polarisation position angle (PA) swing (Radhakrishnan V and Cooke DJ 1969). Simulations (Foster G. *et al.* 2015) show that the polarisation characteristics of the pulsar can be utilised to enhance the ToA estimation. An estimate of a telescope's instrumental responses can be obtained from full-polarisation observations of known bright pulsars. By employing polarimetric data, the ToA estimates can be improved (Susarla S.C. *et al.* 2025; Guillemot Lucas. *et al.* 2023).

The Gauribidanur radio observatory facilitated single-polarisation pulsar observations across a 1.5 MHz band at a centre frequency of 34.5 MHz (Deshpande A. A. and V. Radhakrishnan. 1992) and also between 60 and 80 MHz (Bane Kshitij S. *et al.* 2024). The current work enables instantaneous 16 MHz-wide dual polarised pulsar observations between 130 and 350 MHz using the GBD-DART pulsar array [Pandian,2025 in review].

The design details of the GBD-DART and its capabilities to observe solar transients and pulsars are given in [Pandian,2025 in review]. In this paper, we provide details of the newly developed pulsar observing capabilities and the results from observing a set of bright pulsars in a full polar mode.

**Author for correspondence:** Arul Pandian B, Email: arulpandian022@gmail.com  
**Cite this article:** Author1 C and Author2 C, an open-source python tool for simulations of source recovery and completeness in galaxy surveys. *Publications of the Astronomical Society of Australia* **00**, 1–12. <https://doi.org/10.1017/pasa.xxxx.xx>

The LOFAR, LWA, and MWA telescopes use specific pulsar processing pipelines based on PSRCHIVE and Presto utilities (Stappers B. W. *et al.* 2011; Bondonneau Louis. *et al.* 2021; Stovall K. *et al.* 2015; Bhat N. D. R. *et al.* 2023; Yu Ting. *et al.* 2025; Ransom S. 2011). The current work uses a combination of custom-developed Python scripts for data capture and PSRCHIVE and Presto modules for near-real-time data reduction and archive generation.

## 2. Pulsar Signal Processing

We present a brief overview of the array architecture and the signal conditioning in this section.

### 2.1. Overview

An overview of the GBD-DART antenna array signal chain is given in Figure 1. The array as outlined in Section 2.2 consists of 32 off-axis dual-polarised LPDAs configured as a diamond-shaped tile. The RF signals from each polarisation are suitably amplified and combined independently to create a voltage beam towards the zenith. Then the combined signals are further amplified and transmitted as optical signals to the observatory lab, located 300 metres away, where they are converted back to RF signals. Details of the analogue front-end system are presented in Section 2.3. The RF signals are then band-limited to 16 MHz using a set of band-pass filters, translated to an IF band in a heterodyne receiver, and band-pass sampled with a 33 MHz sampling clock. Further details of this system are presented in Section 2.4.

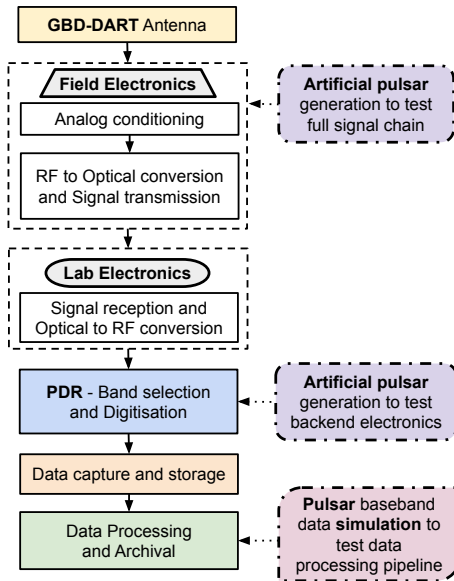


**Figure 1.** GBD-DART Signal Chain, data flow, and testing provisions of the pipeline.

Sampled data is packetised and sent through Ethernet to a data recording system. The data recording system incorporates transient buffers, data recording, and health monitoring features. During a pulsar observation, the transient buffer data is passed to a data processing system, where the recorded data is processed immediately after each observation using a combination of custom and standard pulsar data reduction utilities. The reduced archives after processing are subsequently backed up to a remote storage

system, while the raw data (approximately 220 GB per hour of observation) is not retained. Further details of this data processing are presented in Sections 2.5 and 2.6.

The receiver chain also incorporates tools to generate artificial pulse signals, aiding in the diagnosis of critical pipeline stages. The use of artificial signal generation is described later in section 3.

### 2.2. Antenna Array

GBD-DART is a diamond-shaped array formed out of 64 log-periodic dipole arrays (LPDA) positioned in a checker-board layout. The LPDAs are grouped in four, with opposite pairs slightly tilted toward each other, thus forming a pyramid shape. This primary configuration provides dual-polarised outputs with a half-power beam-width (HPBW) of between 60 and 70 degrees for the 130 and 350 MHz bands when the signals from the opposite pairs of LPDAs are combined. The pyramids have a maximum baseline of 7 meters in the array. The signals from the pyramids are combined in a tree fashion to give the array gain of approximately 22 dBi at 200 MHz (about 15 degrees HPBW).

### 2.3. Analog Front-end

A current BALUN arrangement feeds each LPDA output through a low-noise amplifier (LNA). The LNAs provide 20 dB of gain and are fitted with a high-pass filter at the inputs to reject out-of-band signals below 130 MHz, and a Bias-T network at the LNA outputs to feed a DC supply to the LNAs.

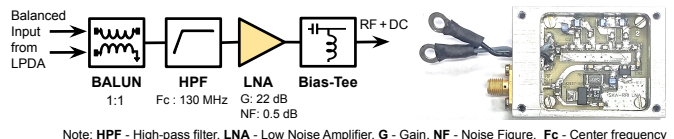


**Figure 2.** Differential signals from the LPDA are fed to the Low Noise Amplifier via a BALUN. The amplifier inputs are fitted with a high-pass filter to reject frequencies below 130 MHz. The low noise amplifier module has a gain of 20 dB and a noise figure of 1.35 dB.

Since the LNA outputs are to be combined to form a phased array output, the individual LNA gains are matched, the phases of the LNAs, interconnecting cables, and combiners are aligned to be within about  $\pm 5^\circ$ . The voltage sum from the two polarisations (32 LPDAs each) is routed to a high-fidelity analog signal conditioning front-end module, the Tubular Receiver.

The Tubular Receiver, as outlined in Figure 3, consists of three filters, three amplifiers and four attenuators that are interleaved suitably to yield a gain of about  $51 \pm 0.5$  dB between the 120 to 350 MHz band.

The amplified signals from the Tubular Receiver are routed to an electrical-to-optical converter module, which transmits the two polarisation radio bands as an optical amplitude-modulated signal at 1310 nm through a single-mode fibre to the observatory electronics lab, a distance of 350 m. The optical signals are converted to electrical signals at the observatory electronics room and fed to a portable digital receiver back-end for digitisation and recording.

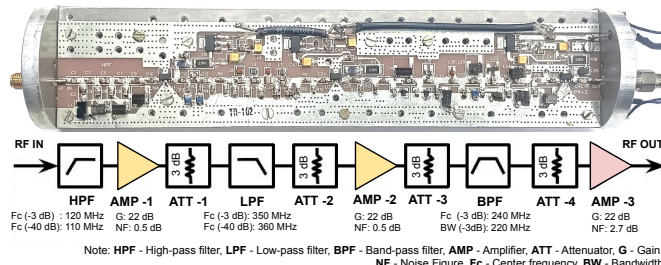


**Figure 3.** Picture show the analog conditioning module, the Tubular Receiver circuit board and its functional blocks. It consists of three stages of filtering (HPF, LPF and BPF) and three stages of amplifiers (AMP-1 to AMP-3). The filters are preceded and followed by a 3 dB attenuators to maintain operational stability.

#### 2.4. Analog and Digital Back-end

The analog and digital back-end, as outlined in Figure 4, is a portable dual receiver (PDR) with two-channel 16-MHz wideband heterodyne receiver cum digitiser (Vinutha C. *et al.* 2017). It can select a contiguous 16 MHz band from the 130 and 350 MHz span, using a suitable local oscillator frequency. The local oscillator clock for the mixer stage of the receiver is generated using an HP synthesizer. An outline of the RF and the IF internal sections of PDR is given in appendix, Figure 26. The sampling clock for the digitiser is generated using a DLL in the FPGA. Both the HP synthesiser and the FPGA receive a 10 MHz reference clock generated from a Trimble make GPS unit. A 1-PPS signal from the Trimble synchronises start of data flow from the receiver. The PDR has two 8-bit digitisers sampling the two polarisation signals at 33 MSPs. The sampled data from the two digitisers are time-tagged, packaged into a UDP packet, and transmitted via Ethernet ports to a data acquisition system (DAS). The PDR uses analog device ADCs for digitisation, and an Xilinx Virtex-5 FPGA for packetising the sampled data and transmitting time-tagged data packets over a Gigabit Ethernet port.

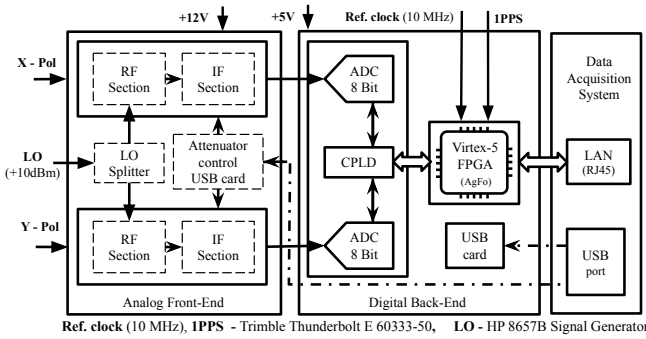


**Figure 4.** The portable dual receiver (PDR) is a two-channel, 16-MHz-wideband heterodyne receiver and digitiser.

#### 2.5. Data Capture

The UDP packets arriving from the PDR are captured in the ramdisk by the data acquisition system (DAS) using the GULP utility (Corey Satten. 2008). The GULP writes out the UDP packets in a PCAP format (Harris G. *et al.* 2025). The DAS maintains three ring buffers of sizes 10, 20, and 70 GB to facilitate the smooth transfer of observation data from Ethernet to the spectrum monitoring and transient data recording processes. A set of dedicated buffer management routines orchestrates the data copying

tasks across the buffers. The 10 GB ring buffer (the GULP buffer) eases the arrival of UDP packets by accumulating them in 2 GB-sized files, once every 30 seconds, corresponding to a 2x33 MSPS data rate.

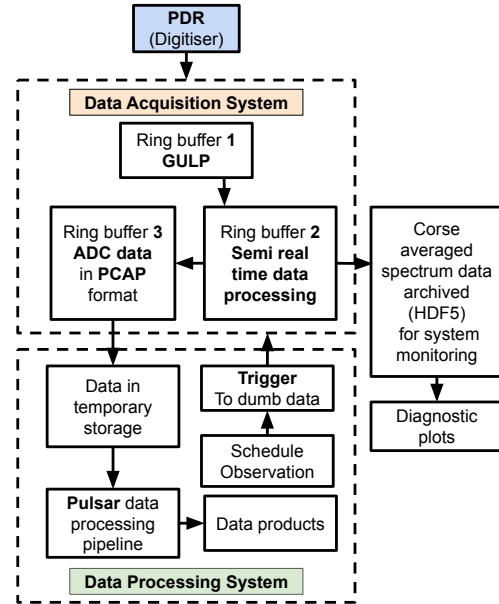


**Figure 5.** Data Capture Architecture

The 2 GB files from the GULP buffer are swiftly transferred to the 20 GB staging buffer, which is then read by a processing task to compute the two self, cross and phased sum products for the two ADC input channels. These products are archived in HDF5 format in the DAS server with a spectral resolution of 64.5 kHz and a time resolution of 1 s, and are continuously recorded 24/7 to monitor the system's performance. The data from the 20 GB ring buffer is also copied to the 70 GB buffer, also known as a transient buffer. The role of the transient buffer is to always maintain the last 5 (or programmable number of) minutes of raw data (10x2 GB) files so that an observation for a pulsar or a transient source such as an FRB could be carried out instantly when a trigger is received from an external system. During a pulsar observation, a trigger is sent to the DAS. Upon receiving the trigger command, the DAS PC would send a programmed number of 2 GB files ( 120 for an hour-long observation) from the transient buffer to an external PC through a Gigabit Ethernet port. The DAS PC connects to the PDR through a dedicated 1-Gigabit Ethernet port to facilitate streaming data flow. An outline of this data capture architecture is outlined in figure 5.

#### 2.6. Pulsar Data Processing

The digitised observation data acquired with GULP is in a PCAP format. A Python script was used to count the packets and remove the PCAP header from the UDP packets. Each data packet will contain 512 samples, alternating between the two channels. Time series data were written in the DADA (van Straten. W., 2021) format, with the first 4096 bytes containing the observation settings. Depending on the choice of data processing, single-polarisation or full-polarisation data can be written out. Multiprocessing (McKerns M.M. *et al.* 2012) libraries from Python were used to accelerate the DADA conversion. As shown in Figure 6, data was processed in coherent de-dispersion with DSPSR (van Straten.

W. & Bailes. M. 2011) and DIGIFITS, which is part of DSPSR, to generate total-intensity and full stokes search mode PSRFITS. further data can be used to perform Incoherent de-dispersion and single pulse search. Coherent de-dispersion mode, dsspr performs a long FFT depending on the given dispersion measure (DM) of the pulsar and deconvolves the response of the interstellar medium, then performs IFFT. This time series data was again Fourier-transformed using a given number of FFT points, and the power spectra were averaged and folded with pulsar periods from the given ephemeris file taken from the ATNF pulsar catalogue (Hobbs. G. et al. 2004).

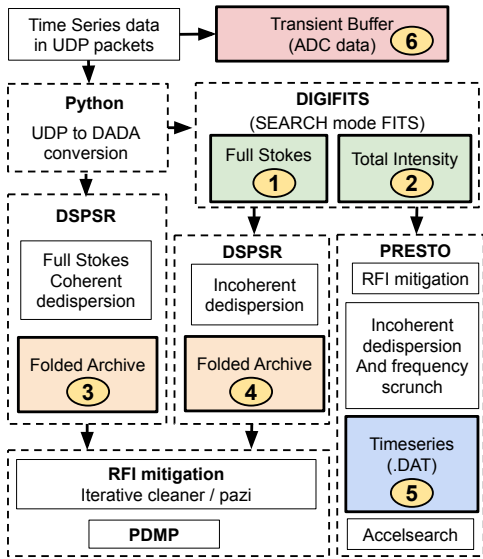


Figure 6. Pulsar Data processing pipeline

DSPSR performs Incoherent de-dispersion and folding on the filter-bank data generated by *digifil*. Another copy of the filter-bank data is processed by PRESTO (Ransom S. 2011) utilities. The *rfifind* was used to perform RFI mitigation, *prepdata* and *accelsearch* were used to de-disperse, frequency scrunch and search for pulsar candidate in the data. *Prepfold* utility was used to fold the pulsar candidate and predict the period and period-derivative of the pulsar. PSRCHIVE utilities (Hotan A. W. et al. 2004) were used to inspect the Folded archive in FITS format. The iterative cleaner and *pazi* were used to perform RFI cleaning in fits files. The cleaned archives are used to search in period, period-derivative and DM space to estimate best values using *pdmp*.

### 3. System Validation

The new pipeline was validated with artificial pulsar signals. A test setup, as outlined in Section 3.1, was used to study the instrument's dynamic range and to determine a linear operating range suitable for pulsar observations. Similarly, fake pulsar polarimetric data, as described in Section 3.2, was generated and used to validate the full polar pulsar data reduction software pipeline developed.

#### 3.1. Validation with Emulated Pulse Signals

A pulsed signal generator (Abhishek R and Sathish R. 2025), as shown in Figure 7, built based on two noise sources, an RF switch,

a power combiner, and a *Raspberry Pi*, was used to generate artificial pulsar signals. The Raspberry Pi module's role is to receive a one-pulse-per-second (1PPS) signal from a GPS and initiate the pulse generation by controlling the duty cycle of the RF switch. The instrument setup allows on- and off-pulse power levels to be varied over a broad range to study the recovered SNR from the system.

The two noise source signals combine during the on-pulse period (when the RF switch is ON), determining the pulse width and pulse power. The second noise source (2) signal, which is always present, determines the off-pulse power. During the study, the off-pulse power was manually set to -70 dBm, and the on-pulse power was varied around -70 dBm using the variable attenuator in 3 dB increments over a 50 dB range, while maintaining a constant pulse width of 100 ms and a pulse repetition period of 1 s.

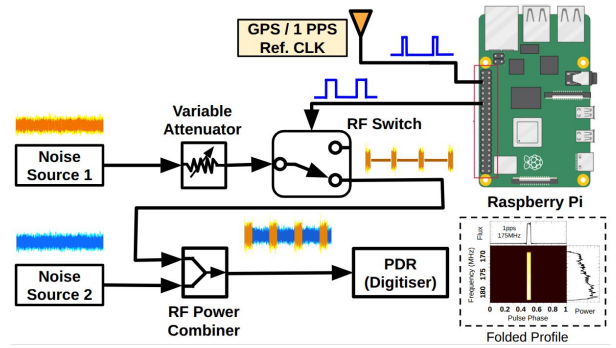


Figure 7. Pulsar emulation signal flow.

The artificial pulse signals for the different pulse-power settings were passed through the analogue chain and then into the PDR for digitisation and recording. The data collected over 100 seconds for each setting were Fourier-transformed and then averaged by folding at the 1s pulse period across a fixed number of bins using standard pulsar processing tools. Figure 8a shows the relationship between the input noise power (RF input power: sum of two noise source signals) fed to the analog chain and the power at the IF output fed to the digitiser, reflecting the observed linearity. The SNR observed in the folded pulses for each of the input pulse power settings is shown in Figure 8b, reflecting the consistency after digitisation.

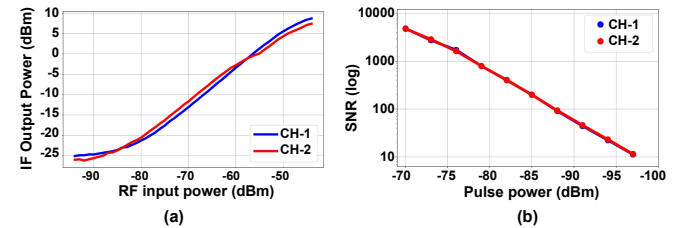
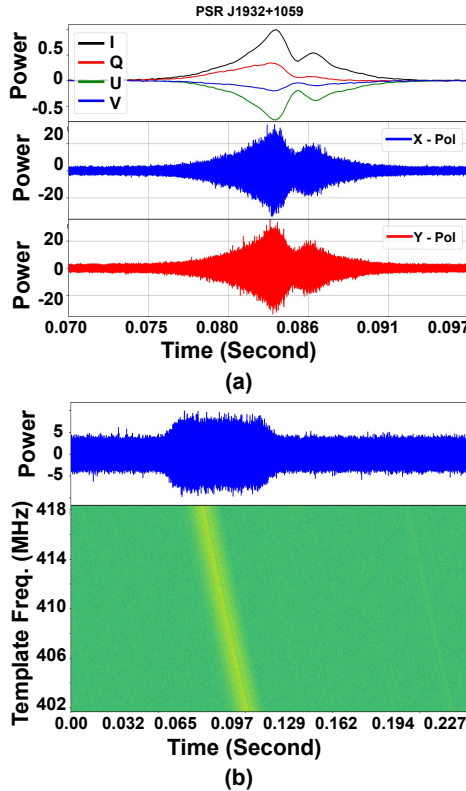


Figure 8. (a) PDR linearity test to find optimum operating RF power. (b) SNR linearity test on PDR channels with emulated pulsar signal shown in Figure 7.

This test was also repeated on each RF path, including the RF optical modules, to verify their consistency and efficiency in processing pulsed signals.

### 3.2. Validation with Simulated Pulse Polarisation

We studied the consistency of the software pipeline for measuring polarised signals using simulated signals. We used the Stokes pulse profile from the EPN catalogue as a template (Gould D.M. and A.G. Lyne. 1998) to obtain the constituent amplitudes and phase differences required for the X- and Y-polarisation voltage signals of the measured coherence.



**Figure 9.** Polarised pulse simulation, (a) On pulse full stokes PSRFITS template profile of J1932+1059 pulsar at 410 MHz (top panel), Computed time series of the X - polarisation (middle panel), Computed time series of the Y - polarisation (bottom panel). (b) Dispersed time series of the X - polarisation.

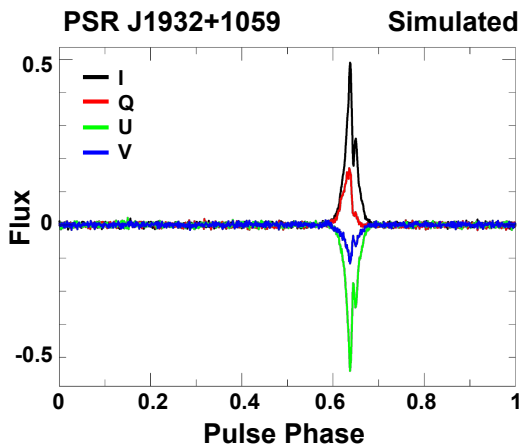


**Figure 10.** Pulse profile recovered by the pipeline after processing the simulated EPN B1929+10 profile data shown in figure. 9.

Random integers were generated as 8-bit ADC samples with 4 sigma level using Numpy (Harris C. R. *et al.* 2020). These samples are created with a rate of 33 MSPs, the same as the digitiser's sampling rate. The pulsar profile with complete Stokes information was used from the EPN pulsar catalog. A 1024-bin profile from the EPN catalogue was interpolated to yield 33 noise samples.

To create timeseries voltage samples, this 2-D template was utilised in conjunction with the *Noise generator* package from *baseband-tasks* (Marten van Kerkwijk. *et al.* 2025b). These samples are later dispersed using the *Disperse* package from *baseband-tasks*. Numpy (Harris C. R. *et al.* 2020) was used to scale dispersed timeseries data to integers, produce 8-bit ADC samples with a 4 sigma level, and write out in a *DADA* format *baseband* (Marten van Kerkwijk 2025a).

This voltage time series was dispersed for our study by using the catalogued 410 MHz DM, shown in Figure 9b. In Figure 9a, the Template full-Stokes pulsar profile is shown in the top panel. The middle and bottom panels show the X- and Y-polarisation voltage time series generated from the coherence product of the template data.

The simulated data were analysed using the processing pipeline to generate the polarisation end products shown in Figure 10 that match well to the EPN profile.

### 3.3. Validation of Signal Integrity

The signal processing pipeline of the DART system (B Pandian, 2025) hardware modules were verified for signal integrity before commencing the regular pulsar observations. We highlight here several key factors that were taken into account.

The DART antenna elements are designed in an off-axis configuration with a 23-degree zenith tilt, resulting in approximately twice the gain of a single LPDA with the same physical area. The low-noise amplifier (LNA) and the balun are mounted at the antenna feed point to avoid resistive losses, which are crucial to determining the receiver chain's noise floor. Individual LNAs are tuned and phase-matched to the reference LNA to minimise signal loss during phased addition. We have used LMR-195 RF cable, which is certified for outdoor use and UV-resistant. Each cable was precisely cut, manually crimped, and tested for attenuation and phase match. The 8-way and 4-way power combiner was designed with ADP-2-1W RF power combiner chips and phase-matched to combine all 64 LPDAs of the array in two stages. From LNA to the power combiner, we have maintained the phase coherence with the tolerance of  $\pm 5$  degrees.

In the field, analog conditioning was performed using an analog tubular Rx, which consists of high-pass and low-pass filters and three-stage high-gain amplifiers, as shown in Figure 3. The amplified RF signal was sent through the RFoF modules, which are enclosed in aluminium boxes that provide RF shielding. An RF signal leakage test was conducted between the X-pol and Y-pol channels using an artificial pulse generator setup to verify that better than -20dB isolation is achieved. The dynamic range of the analog and digital receivers was estimated using a linearity test. To avoid unwanted pickup and improve the isolation of the digitiser, we have replaced RG174 with higher-shield semi-flex cables in the PDR analog sections. The power supply of the PDR digitiser was changed from an SMPS to a linear supply to avoid switching noise on the power rails. A GPS-disciplined 1PPS and 10 MHz reference clock generator (Trimble Thunderbolt E 60333-50) was used to lock the HP 8657B Signal Generator, which served as a

local oscillator (LO). The HP 8657B Signal Generator was tested with a frequency counter to verify the accuracy of the clock.

To ensure we do not lose the data during streaming UDP Ethernet transfers, we have used a RAM disk as a ring buffer to handle the incoming data rate (66MSPs). A three-stage RAM-disk ring buffer was used to process array monitoring data in parallel.

#### 4. Results and Discussions

This section presents results from observing five pulsars. The data presented here were obtained in full Stokes mode of observation, using the IAU convention for polarimetric observations. Polarisation calibration of the data was performed for the receiver response using the *pac* package from PSRCHIVE. An instrumental calibration solution was obtained by feeding an artificial pulsed noise signal at the first-stage analog receiver in the field.

##### 4.1. J0953+0755

PSR J0953+0755 (B0950+08) appears to be a solitary pulsar with a period of 253.07 milliseconds and a low dispersion measure of  $2.969 \text{ pc/cm}^3$ . This pulsar is one of the brightest and most highly polarised, and it is routinely studied for giant pulses, single-pulse variability, and its intrinsic polarisation properties to better understand the radio emission region and provide constraints on the pulsar model (Tan T.Z. *et al.* 2025). In Figure 11a, we present a high SNR average pulse (AP) profile and pulse intensity across the frequency from one of our 40 minutes of observation. The fraction of polarisation with position angle is shown in Figure 11b.

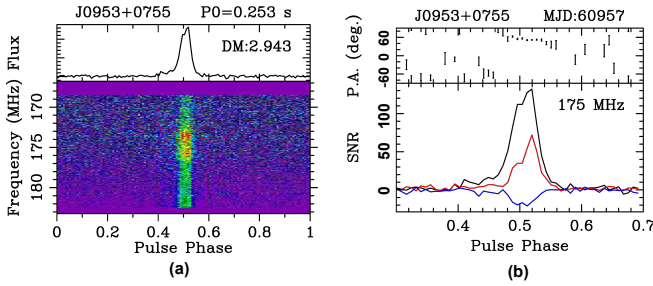


**Figure 11.** Pulse profile of J0953+0755. (a) Pulse intensity across the frequency. (b) Polarisation fraction, total intensity (Black), linear polarisation (Red), circular polarisation (Blue).

In low-frequency radio observations, this pulsar is being studied extensively to investigate the effect of interstellar scintillation on pulse profile variability over frequency (Shabanova T.V. and Shitov Y.P. 2004; Ziwei Wu. *et al.* 2022). In Figure 12a, we have presented the estimated rotation measure (RM) in a span of 100 days from our data. The *rmfit* package from PSRCHIVE was used to calculate the RM. Figure 12b illustrates RM measurement being  $3.08 \pm 1.14 \text{ rad/m}^2$  for MJD 60994.

The pulse amplitude of this pulsar was highly variable and known for generating high-intensity giant pulses with a factor of more than 200 (Smirnova T.V. 2012).

The high-intensity giant pulses from this pulsar were studied for microstructure analysis in the pulse region and to understand the pulse emission mechanism. The morphologies and spectral structure of the pulse were compared with those of FRB and magnetar signals to understand the propagation effects of the source environments (Bilous A.V. *et al.* 2022). We observed this pulsar

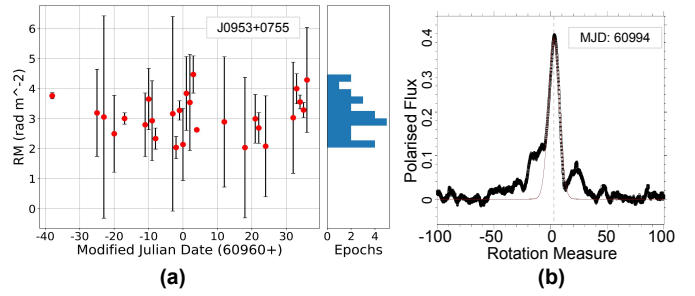


**Figure 12.** J0953+0755 Rotation measure estimation using *rmfit*. RM =  $3.08 \pm 1.14 \text{ rad/m}^2$

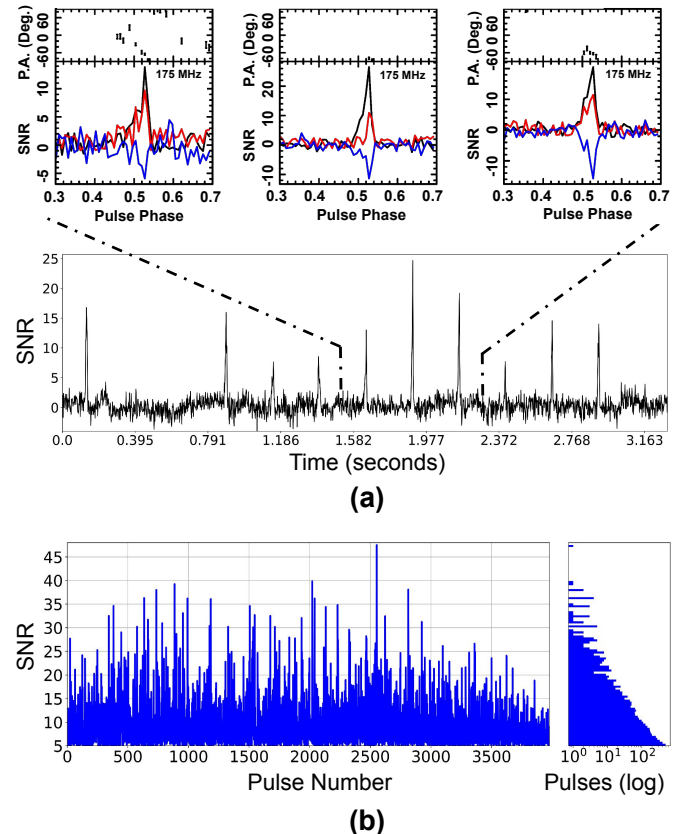


**Figure 13.** (a) Three bright single pulses plotted with linear polarisation (Red), Circular polarisation (Blue) [top panel], Single pulse train of 3 second data [bottom panel], (b) 3978 pulses detected above 5 sigma from the J0953+0755 in 40 minutes of observations at 175 MHz on MJD 60994 (which is routinely observed by the array). Single pulses were detected at 175 MHz from the observations.

on MJD 60994 with an SNR of 300. *single\_pulse\_search.py* package from the PRESTO was used to conduct a single pulse search on this data and detected 3978 single pulses above an SNR of 5, as shown in Figure 13b. Frequency scrunched time series data of 3.2 seconds with polarisation plot for three consecutive giant single pulses are also demonstrated in 13a.

Based on the giant pulse event time, the 253-ms length of search mode data was sliced and plotted against frequency with and without de-dispersion, as shown in Figure 14. This work illustrates the features of the processing pipeline for handling and searching radio transients in the observation data.

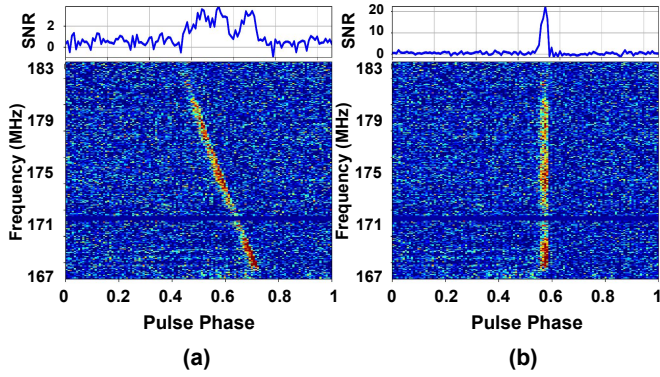


Figure 14. J0953+0755 Single pulse before and after dispersion correction.

#### 4.2. J0534+2200

The Crab pulsar (PSR B0531+21 or PSR J0534+2200) is a much-studied, young, and energetic pulsar with a period of 33 milliseconds and a dispersion of  $56.75 \text{ pc}/\text{cm}^3$ . It is radio-bright, with a spin-down rate  $-3.77535 \times 10^{-10} \text{ s}^{-2}$  and a flux density of 8 Jy at 150 MHz. The pulsar is routinely observed to study the giant pulses, nanoshots, and spin period glitches (Singha J. *et al.* 2022) it generates. At low frequencies, pulses are scattered, providing a handle to estimate the interstellar medium model (Kirsten F. *et al.* 2019). This pulsar is located at the northern edge of the tile beam, and it has been routinely detected in our observations with SNRs 10 to 16. We have observed this pulsar at 175 MHz and presented the AP profile with intensities across the frequency in Figure 15a. The amount of polarised intensities measured against pulse phase is shown in Figure 15b.

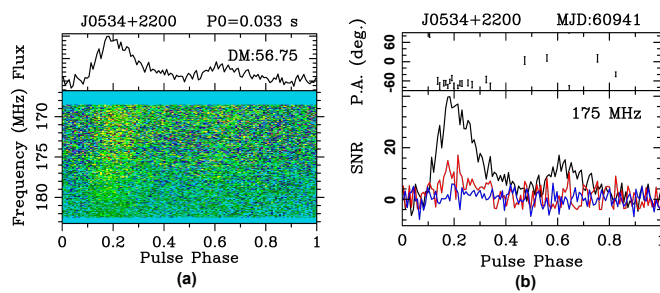


Figure 15. Pulse profile of J0534+2200 (CRAB Pulsar). (a) Pulse intensity across the frequency. (b) Polarisation fraction, total intensity (Black), linear polarisation (Red), circular polarisation (Blue).

Faraday rotation of this pulsar has been measured using polarisation properties, and an RM of  $-40.5 \text{ pm} 4.5 \text{ rad/m}^2$  is reported (Manchester R. N., 1971). The polarisation variation of this pulsar was used as a probe to study the magnetic field environment of the host nebula over a decade (Rankin Joanna M. *et al.* 1988).

Figure 16a presents the Faraday rotation measured for this pulsar over 100 consecutive days in our observation. One of the epoch's *rmfit* estimate profile is shown in 16b. The average rotation measure (RM) for the 100 epochs is estimated to be  $-39.4 \pm 1.8 \text{ rad/m}^2$  in this work.

The giant pulses from this pulsar were used for scintillation studies and found to be heavily affected by Kolmogorov turbulence at higher frequencies, which is crucial for placing constraints on the FRB-like searches at higher frequencies (Doskoch G.M.

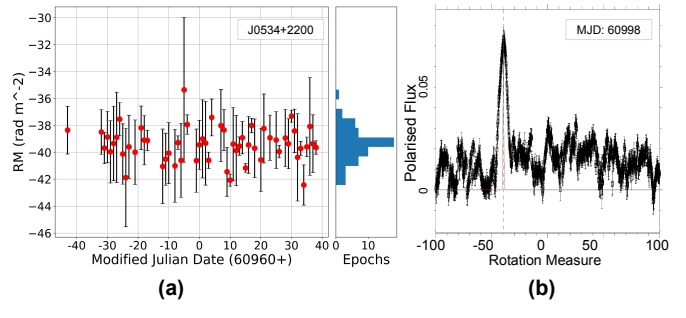


Figure 16. J0534+2200 Rotation measure estimation using *rmfit*. RM =  $-39.4 \pm 1.8 \text{ rad/m}^2$

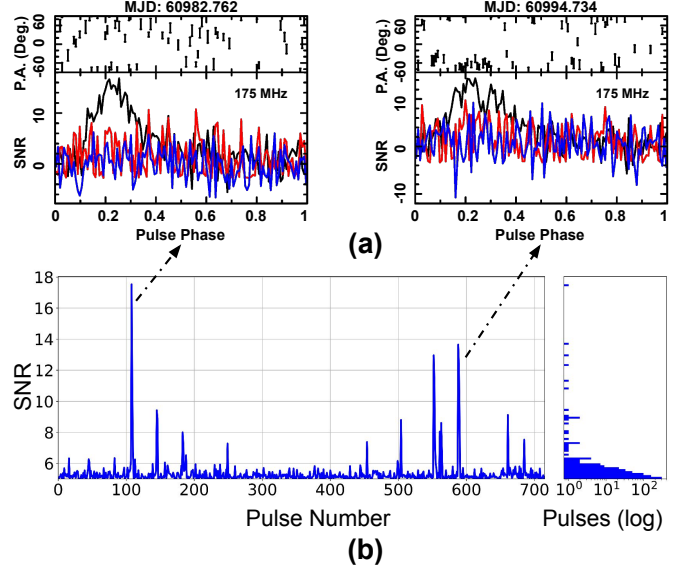


Figure 17. (a) Two bright single pulses plotted with linear polarisation (Red), Circular polarisation (Blue), (b) 706 Pulses detected above 5 sigma from J0534+2200 in 11.3 hours observations at 175 MHz spanning 18 days which is routinely observed by the array. J0534+2200 Single pulses detected at 175 MHz from the observations.

*et al.* 2024). Our observation at 175 MHz over 11.3 hours spanning 18 days in November 2025 detected giant pulses with SNR greater than 5 at a rate of about 1 per minute. Figure 17b shows the counts of detected giant pulses as a function of their SNR. The fractional polarisation measured for two of the giant pulses is shown in Figure 17a.

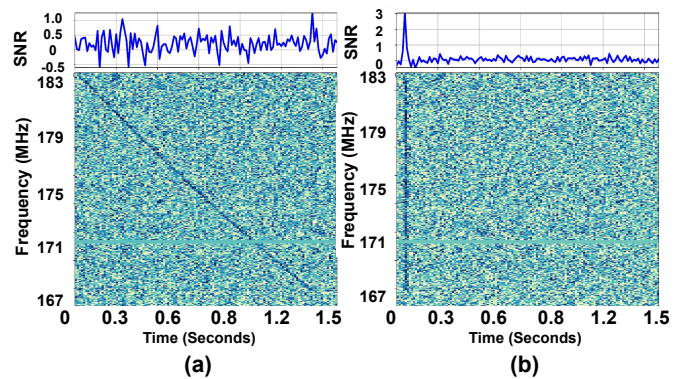
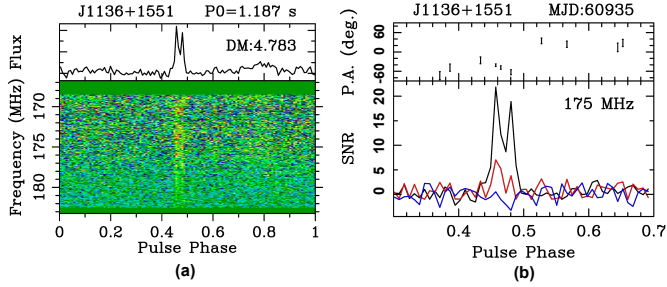


Figure 18. J0534+2200 Single pulse before and after dispersion correction.

High-dispersion pulsar signals experience more delay in low-frequency observation. One of the GP of crab pulsar takes almost 1.5 seconds to cross our band of observation, shown in Figure 18a—the expected improvement in SNR after de-dispersion was shown in Figure 18b. The effect of dispersion at low frequencies can be beneficial when searching for high-DM FRB signals.

#### 4.3. J1136+1551

PSR J1136+1551 (B1133+16) is a normal pulsar with a period of 1.19 seconds and a dispersion measure of  $4.841 \text{ pc}/\text{cm}^3$ . This pulsar is an isolated, mode-changing pulsar. It has a complex average profile with two well-separated main components, whose component widths change with frequency, a phenomenon known as radius-to-frequency mapping (RFM) (Oswald Lucy. *et al.* 2019).



**Figure 19.** Pulse profile of J1136+1551. (a) Pulse intensity across the frequency. (b) Polarisation fraction, total intensity (Black), linear polarisation (Red), circular polarisation (Blue).

Figure 19a presents the AP profile with pulse intensities as a function of observation frequency. The corresponding epoch's polarisation fraction of the pulse is shown in Figure 19b.

This pulsar exhibits a sub-pulse drift mode with the bright single pulse emission (Tan Jun. *et al.* 2024) and scintillation (Ziwei Wu. *et al.* 2022). It shows a much larger intensity modulation at low sky frequencies, resulting in narrow, bright emissions that may provide a vital clue to understanding the underlying mechanism of bright-pulse emission (Karuppusamy R. *et al.* 2011).

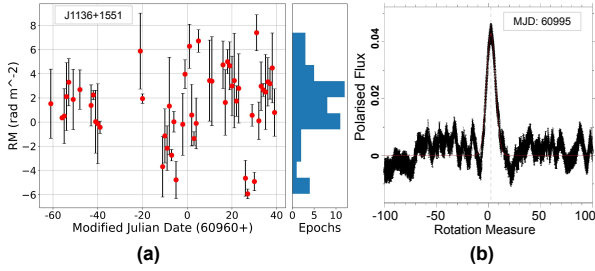


**Figure 20.** J1136+1551 Rotation measure estimation using rmfit.  $1.42 \pm 1.9 \text{ rad/m}^2$

Rotation measure of this pulsar was measured over 100 days of observation, and it was found to vary as shown in Figure 20a. The rmfit profile of one of the high SNR epochs is shown in Figure 20b.

The occurrence of unusually intense single pulses provides a sample of instances in which we can observe frequency evolution along field lines in the magnetosphere, allowing us to develop a description of the shape of the active emission region and build

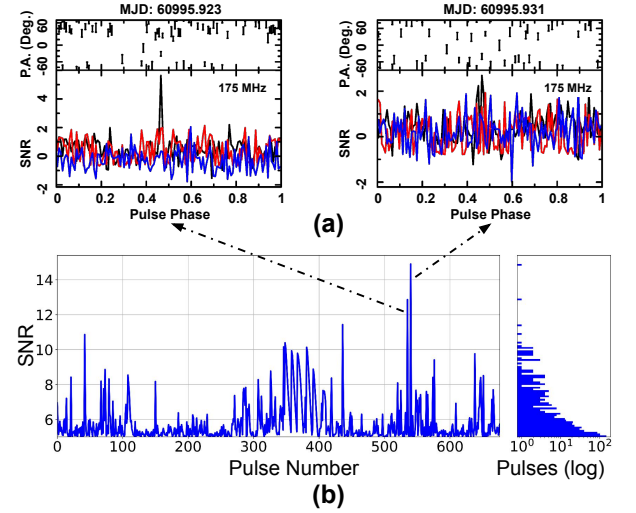


**Figure 21.** (a) Two bright single pulses plotted with linear polarisation (Red), Circular polarisation (Blue), (b) Single pulse detection of PSR J1136+1551 with S/N more than 5.

constraints on models of the emission region within the magnetosphere (Oswald Lucy. *et al.* 2019). We have conducted a single pulse search in our November 2025 dataset, and found around 690 bright pulses above SNR 5 as shown in Figure 21b. Two of the bright pulses shown in Figure 21b, and their total intensity pulse profile was different despite their close occurrence.

#### 4.4. J0837+0610

PSR J0837+0610 (B0834+06) is an isolated pulsar with a period of 1.27 seconds and a dispersion measure of  $12.864 \text{ pc}/\text{cm}^3$ . This pulsar profile has two close pulse components within 10 degrees of pulse longitude, which is also growing towards higher frequencies (Johnston S. 2008).

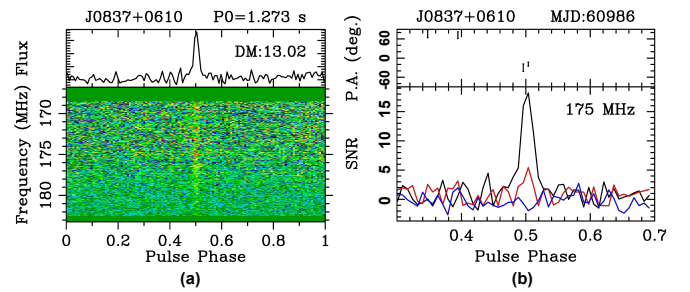


**Figure 22.** Pulse profile of J0837+0610. (a) Pulse intensity across the frequency. (b) Polarisation fraction, total intensity (Black), linear polarisation (Red), circular polarisation (Blue).

It exhibits a nulling pulse phenomenon with a fraction of 7–9% (Ritchings R.T. 1976; Wang P.F. *et al.* 2020). The scintillation parameter of this pulsar was studied, and the scattering screen distance was reported in the frequency range 145–155 MHz (Ziwei Wu. *et al.* 2022).

In our observation, this pulsar is detected with an average SNR of 15. Figure 22a, presents the AP profile against observed flux density across the frequency band. The fraction of the polarisation seen in the profile is plotted in Figure 22b.

#### 4.5. J1921+2153

PSR J1921+2153 (B1919+21) is a pulsar with a 1.34-second period and a dispersion measure of  $12.444 \text{ pc}/\text{cm}^3$ . The rapid change in the fraction of polarisation leads to orthogonal mode jumps in the PA swing and component blending across frequency (Johnston S. 2008). The fluctuation spectral analysis of PSR J1921+2153 at 618 MHz revealed a jump in the phase variation across the pulse components, categorised as switching phase-modulated drifting (Basu R. *et al.* 2019). The high time resolution of full polar data was used to study linear polarisation position angle and found that it follows the RVM model (Johnston S. *et al.* 2024).

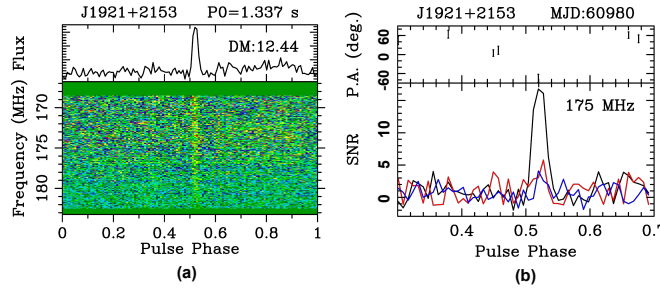


**Figure 23.** Pulse profile of J1921+2153. (a) Pulse intensity across the frequency. (b) Polarisation fraction, total intensity (Black), linear polarisation (Red), circular polarisation (Blue).

Most detailed studies of pulsar properties require polarimetric observations. In Figure 23a, we are showing the AP profile from our observation with spectral intensity across time. The corresponding data was plotted with fraction of polarisation in Figure 23b.

#### 4.6. RFI Mitigation

Radio frequency interference (RFI) has a significant impact on pulsar observation. Pulsars are weak sources; therefore, RFI is prevalent and reduces the pulse profile's signal-to-noise ratio (SNR). To get a high SNR, we may have to perform RFI cleaning. In our pipeline, we have adopted the RFI removal tool for pulsar archives *Iterative cleaner* (Lars Kunkel. 2017), which is based on the surgical cleaner included in the *coast\_guard* (Lazarus P. *et al.* 2020) pipeline.

#### 4.7. Current status

For pulsar observations, instrument stability is essential. Two crucial challenges are managing the high data rate and maintaining clock stability over time. The array is routinely monitoring five bright pulsars. Figure 24 shows observation status for five pulsars with observed epoch and corresponding SNRs detected from the analysis. Our observations collect approximately 1.2 TB of data and process it each day on an AMD R9 desktop server. We have a GPS-synchronised clock as a reference system for the backend systems.

The Crab pulsar is one of the regularly observed sources in the array; we report here its spin-down obtained over nearly 200 days of observation. The estimated spin period of PSR J0534+2200, as determined using *PDMP* over approximately 200 days, is plotted against MJD in Figure 25. We utilised the Jodrell Bank Observatory (JBO) CRAB pulsar monthly ephemeris data (Lyne

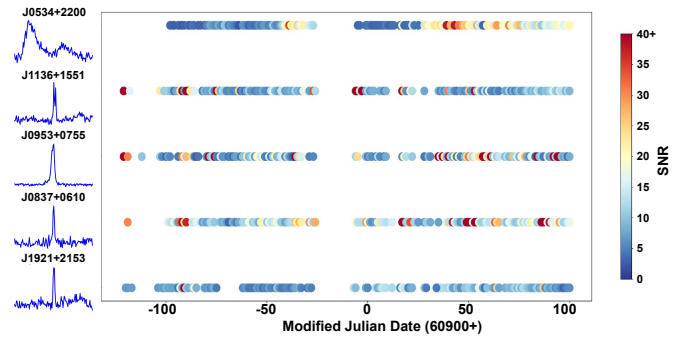


**Figure 24.** Pulse profiles, observation epochs and the detected SNR for the five bright pulsars routinely observed from MJD 60820 to 61000 by the GBD-DART array.

A.G. *et al.* 1993) to verify the spin-down trend line of the spins, which closely match at the first order with our estimates.

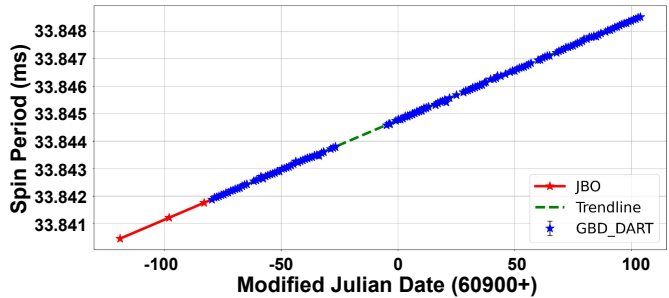


**Figure 25.** Spin period of PSR J0534+2200 estimation from our observation between MJD 60820 and 61000 (Blue). Monthly ephemerides data for this pulsar from JBO (Red) and extended trend line from the data (green).

#### 5. conclusion

We have developed a new pulsar data processing pipeline for the GBD-DART array. The pipeline consists of both hardware and software modules. In-house-built analog and digital systems are used in the hardware pipeline, and custom-developed Python scripts and standard pulsar tools are employed to implement the various stages of the software pipeline. The entire pipeline was validated with the emulated and simulated pulse signals. The online monitoring feature is incorporated, which provides coarse-averaged data to monitor the array's health. A transient buffer is implemented to transfer raw data upon receiving a trigger for the scheduled pulsar observation and to respond to transient events, such as the FRB detection alert from the Virtual Observatory Event (VOEvent). The pipeline offers coherent and incoherent mode dedispersion. Standard open source RFI mitigation tools were used in this pipeline. We employ an incoherent mode to assess the quantity of good data mitigating RFI (rfifind) in the search-mode fits data. Search-mode data are routinely backed up to facilitate the search for radio transients and single pulses from pulsars. We have presented results from nearly 200 days of observing five bright pulsars: J0953+0755, J0534+2200, J1136+1551, J0837+0610, and J1921+2153. The results include average pulse profiles with polarisation for all the pulsars, results from an RM estimate and a single-pulse study for J0953+0755, J0534+2200, and J1136+1551, and spin-down monitoring results for the Crab pulsar J0534+2200.

Additionally, we have provided the cadence details and SNR for all five pulsars. For archives, we choose to use data formats widely used in the pulsar community. When there is a particular interest, the raw ADC data can also be retained in the DADA format. The data products are stored in folded archives in search mode, in a PSRFITS format compatible with PSRCHIVE. Standard timing tools, such as the tempo and tempo2, can also be used to process the essential information required for pulsar timing. In our observations, CPU multi-threading reduced data processing time nearly in proportion to the observation time. To obtain the intrinsic polarisation characteristics of the pulsar, we have chosen to focus on polarisation calibration in the future. Beam steering, either in analog or digital mode, and broadband observation are planned for the future.

## Disclosures

The authors declare there are no financial interests, commercial affiliations, or other potential conflicts of interest that have influenced the objectivity of this research or the writing of this paper.

## Conflicts of Interest

None.

## Code, Data, and Materials Availability

The data, materials and software code presented in this article are publicly available in [https://github.com/Arul16psp05/GDARDT\\_lite.git](https://github.com/Arul16psp05/GDARDT_lite.git) at <https://doi.org/10.5281/zenodo.18184048>

## Acknowledgments

We acknowledge the multiple technical consultations with Indrajit Vittal Barve and Shaik Sayuf. We acknowledge the involvement of our colleagues, staffs and security at the Gauribidanur Observatory for their support during the observation, particularly Narendra for the power maintenance. Additionally, we thank the RRI electrical team support on UPS system. We are also grateful to our EEG colleagues for their various forms of support and valuable conversations that aided this work. We thank the Raman Research Institute for supporting this development work. We also thank the Christ University for recognising the research aspect of this effort. Also, we acknowledge the use of RRI library provided access to the Grammarly (Fitria Tira Nur. 2021) tool and publicly available QuillBot (Fitria Tira Nur. 2021) to correct grammar in the manuscript.

## Appendix

### References

Sobey, C and others., (2017). 'Studying Magnetic Fields using Low-frequency Pulsar Observations'. *Proceedings of the International Astronomical Union*, 13, pp. 299–303. DOI: <https://doi.org/10.1017/S1743921317009267>

Foster, R. S. and Backer, D. C. (1990) 'Constructing a pulsar timing array'. *Astrophysical Journal*, 361, pp. 300–308. DOI: <https://doi.org/10.1086/169195>

Edwards, R.T., Hobbs, G.B. and Manchester, R.N., 2006. TEMPO2, a new pulsar timing package—II. The timing model and precision estimates. *Monthly Notices of the Royal Astronomical Society*, 372(4), pp.1549–1574. DOI: <https://doi.org/10.1017/pasa.2023.17>

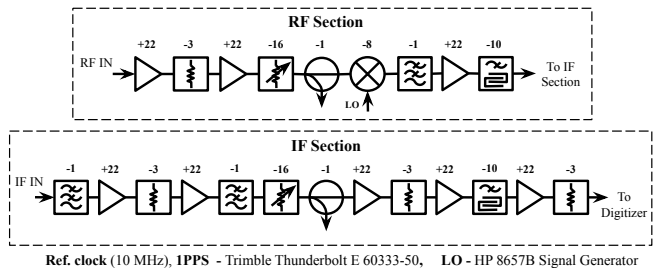


Figure 26. Signal flow of the PDR RF and IF sections

<https://doi.org/10.1111/j.1365-2966.2006.10870.x>

Guillemot, Lucas and Cognard, Ismaël and van Straten, Willem and Theureau, Gilles and Gérard, Eric., 2023. 'Improving pulsar polarization and timing measurements with the Nançay Radio Telescope.' *Astronomy & Astrophysics*, 678, pp.A79. DOI: <https://doi.org/10.1051/0004-6361/202347018>

Krishnakumar, M.A., Manoharan, P.K., Joshi, B.C., Girgaonkar, R., Desai, S., Bagchi, M., Nobleson, K., Dey, L., Susobhanan, A., Susarla, S.C. and Surnis, M.P., 2021. 'High precision measurements of interstellar dispersion measure with the upgraded GMRT', *Astronomy & Astrophysics*, 372(4), 651, p.A5. DOI: <https://doi.org/10.1051/0004-6361/202140340>

Susarla, SC and Johnson, OA and McKenna, DJ and Keane, EF and McCauley, PJ and Verbiest, JPW and Tiburzi, C and Golden, A. (2025) 'Long-term timing results of ecliptic pulsars observed with I-LOFAR', *Astronomy & Astrophysics*, 698, pp. A248. DOI: <https://doi.org/10.1051/0004-6361/202554226>

Radhakrishnan, V and Cooke, DJ, (1969). 'Magnetic poles and the polarization structure of pulsar radiation', *Taylor & Francis*. ADS: <http://adsabs.harvard.edu/abs/1969ApL.....3..225R>

Foster, Griffin and Karastergiou, Aris and Paulin, Remi and Carozzi, TD and Johnston, Simon and van Straten, Willem., (2015), 'Intrinsic instrumental polarization and high-precision pulsar timing', *Monthly Notices of the Royal Astronomical Society*, 453, pp. 1489–1502. DOI: <https://doi.org/10.1093/mnras/stv1722>

Deshpande, AA and Radhakrishnan, V., (1992) 'Pulsar observations at 34.5 MHz using the Gauribidanur Telescope: I', *Journal of astrophysics and astronomy*, 13, pp. 151–165. DOI:<https://doi.org/10.1007/BF02702307>

Bane, Kshitij S and Barve, Indrajit V and Gireesh, Gantyada Venkata Satya and Kathiravan, Chidambaram and Ramesh, Rajaram., (2024) 'Initial results from multi-beam observations of pulsars and solar transient with the digital beamformer for the Gauribidanur pulsar system', *Journal of Astronomical Telescopes, Instruments, and Systems*, 10, pp. 014001–014001. DOI:<https://doi.org/10.1111/1.JATIS.10.1.014001>

Stappers, BW and Hessels, JWT and Alexov, A and Anderson, K and Coenen, T and Hassall, T and Karastergiou, A and Kondratiev, VI and Kramer, M and Van Leeuwen, J and others., (2011) 'Observing pulsars and fast transients with LOFAR', *Astronomy & astrophysics*, 530, A80. DOI:<https://doi.org/10.1051/0004-6361/201116681>

Bondonneau, Louis and Grießmeier, J-M and Theureau, Gilles and Cognard, Ismaël and Brionne, M and Kondratiev, V and Bilous, A and McKee, JW and Zarka, P and Viou, C and others. (2021) 'Pulsars with NenuFAR: Backend and pipelines'. *Astronomy & Astrophysics*, 652, A34. DOI:<https://doi.org/10.1051/0004-6361/202039339>

Stovall, K and Ray, PS and Blythe, J and Dowell, J and Eftekhari, T and Garcia, A and Lazio, TJW and McCracken, M and Schinzel, FK and Taylor, GB., (2015) 'Pulsar observations using the first station of the long wavelength array and the LWA pulsar data archive'. *Astrophysical Journal*, 808, pp. 156. DOI:<https://doi.org/10.1088/0004-637X/808/2/156>

Bhat, NDR and Swainston, NA and McSweeney, SJ and Xue, M and Meyers, BW and Kudale, S and Dai, S and Tremblay, SE and van Straten, W and Shannon, RM and others., (2023) 'The Southern-sky MWA Rapid Two-metre (SMART) pulsar survey—I. Survey design and processing pipeline'. *Publications of the Astronomical Society of Australia*, 40, pp. e021. DOI:<https://doi.org/10.1017/pasa.2023.17>

Yu, Ting and Gong, Hongyu and Gao, Zhifu and Zhang, Zhongli and Wen, Zhigang and Wang, Yujie and An, Tao., (2025) 'A study of 80 known pulsars at 185 MHz using MWA incoherent drift-scan observations'. *Monthly Notices of the Royal Astronomical Society*, 543, pp. 3814–3829. DOI:<https://doi.org/10.1093/mnras/staf1700>

Mamatha T S, Sandhya, Vinutha C, A. A Deshpande. (2017) 'Miniaturised Portable Dual-Channel Receiver for Radio Astronomical Observations'. *RRI dspace*, URL:<http://dspace.rri.res.in/handle/2289/7851>.

Corey Satten. (2008) 'Lossless Gigabit Remote Packet Capture With Linux'. URL:<https://staff.washington.edu/corey/gulp/>.

Guy Harris and Michael Richardson., (2025). 'PCAP Capture File Format'. *Internet Engineering Task Force.*, URL:<https://datatracker.ietf.org/doc/draft-ietf-opsawg-pcap/06/> , libpcap URL:<https://www.tcpdump.org/manpages/pcap.3pcap.html>.

Abhishek R and Sathish R. (2025) 'Artificial PULSAR'. *Github*,. GIT:[https://github.com/Abhishek-R1/Artificial\\_PULSAR.git](https://github.com/Abhishek-R1/Artificial_PULSAR.git).

Marten van Kerkwijk, Jing Luo (Santiago), Chenchong Charles Zhu, Rebecca Lin, Nikhil Mahajan, & P. L. Lim. (2025) 'mhvk/baseband-tasks: v0.4.0 (v0.4.0)'. *Zenodo*,. DOI:<https://doi.org/10.5281/zenodo.15002761>.

Marten van Kerkwijk (2025) 'mhvk/baseband: v4.3.0'. *Zenodo*,. DOI:<https://doi.org/10.5281/zenodo.15001880>.

Lorimer, D.R. and Kramer, M., 2005. Handbook of pulsar astronomy (Vol. 4) *Cambridge university press*. ADS:<https://ui.adsabs.harvard.edu/abs/2004hpa.book....L/abstract>

Gould, DM and Lyne, AG., 1998. 'Multifrequency polarimetry of 300 radio pulsars' *The Royal Astronomical Society*, 301, pp.235–260. DOI:<https://doi.org/10.1046/j.1365-8711.1998.02018.x>.

Tan, TZ and You, XP and Li, JH and Ren, JT and Shi, K., 2025. 'A detailed study on the pulse profile of PSR B0950+08' *Astronomy & Astrophysics*, 701, pp. A102. DOI:<https://doi.org/10.1051/0004-6361/202554636>.

Smirnova, TV., 2012. 'Giant pulses from the pulsar PSR B0950+08' *Astronomy reports*, 56, pp. 430–440. DOI:<https://doi.org/10.1088/0004-6256/144/5/155>

Bilous, AV and Grießmeier, JM and Pennucci, T and Wu, Ziwei and Bondonneau, L and Kondratiev, V and van Leeuwen, J and Maan, Y and Connor, L and Oostrum, LC and others., 2022. 'Dual-frequency single-pulse study of PSR B0950+08' *Astronomy & Astrophysics*, 658, pp. A143. DOI:<https://doi.org/10.1051/0004-6361/202142242>

Shabanova, Tatiana V and Shitov, Yu P., 2004. 'Properties of the linearly polarized radiation from PSR B0950+08', *Astronomy & astrophysics*, 418, pp. 203–211. DOI:<https://doi.org/10.1051/0004-6361:20040058>

Singha, Jaikhomba and Joshi, Bhal Chandra and Bandyopadhyay, Debades and Grover, Himanshu and Desai, Shantanu and Arumugam, P and Banik, Sarmistha., 2022. 'Pulsar timing irregularities and neutron star interior in the era of SKA: an Indian outlook' *Journal of Astrophysics and Astronomy*, 43, pp. 81. DOI:<https://doi.org/10.1007/s12036-022-09874-z>

Kirsten, F and Bhat, NDR and Meyers, BW and Macquart, J-P and Tremblay, SE and Ord, SM., 2019. 'Probing Pulsar Scattering between 120 and 280 MHz with the MWA' *The Astrophysical Journal*, 874, pp. 179. DOI:<https://doi.org/10.3847/1538-4357/ab0c05>

Doskoch, Graham M and Basuroski, Andrea and Halley, Kriisa and Sookram, Avinash and Rodriguez-Ramos, Iliomar and Nahata, Valmik and Rahman, Zahi and Zhang, Maureen and Uhlmann, Ashish and Lynch, Abby and others., 2024. 'A Statistical Analysis of Crab Pulsar Giant Pulse Rates' *The Astrophysical Journal*, 973, pp. 87. DOI:<https://doi.org/10.3847/1538-4357/ad6304>

Rankin, Joanna M and Campbell, Donald B and Isaacman, Richard B and Payne, Robert R., 1988. 'The Crab nebula-Secular variations in the Faraday rotation of the pulsar and the great 1974-1975 scattering event' *Astronomy & Astrophysics*, 202, pp. 166–172. ADS:<https://ui.adsabs.harvard.edu/abs/1988A%26A...202..166R/abstract>

Oswald, Lucy and Karastergiou, Aris and Johnston, Simon., 2019. 'Understanding the radio beam of PSR J1136+1551 through its single pulses' *Monthly Notices of the Royal Astronomical Society*, 489, pp. 310–324. DOI:<https://doi.org/10.1093/mnras/stz2121>

Manchester, R. N., S., 1971. 'Faraday Rotation of the Crab Pulsar Radiation'. *Springer Netherlands*, DOI:[https://doi.org/10.1007/978-94-010-3087-8\\_17](https://doi.org/10.1007/978-94-010-3087-8_17).

Tan, Jun and Wen, Zhi-Gang and Wang, Zhen and Duan, Xue-Feng and Wang, Hong-Guang and Wang, Na and Gajjar, Vishal and Yuan, Jian-Ping and Yuen, Rai and Yan, Wen-Ming and others., 2024, 'The Bright Single Pulse Emission from PSR B1133+16', *Research in Astronomy and Astrophysics*, 24, pp. 045022. DOI:<https://doi.org/10.1088/1674-4527/ad3789>.

TKaruppusamy, Ramesh and Stappers, BW and Serylak, Maciej., 2011, 'A low frequency study of PSRs B1133+16, B1112+50, and B0031-07', *Astronomy & Astrophysics*, 525, pp. A55. DOI:<https://doi.org/10.1051/0004-6361/201014507>.

Johnston, Simon and Karastergiou, Aris and Mitra, Dipanjan and Gupta, Yashwant., 2008, 'Multifrequency integrated profiles of pulsars' *Monthly Notices of the Royal Astronomical Society*, 388, pp. 261-274. DOI:<https://doi.org/10.1111/j.1365-2966.2008.13379.x>.

Ritchings, RT., 1976, 'Pulsar single pulse intensity measurements and pulse nulling' *Monthly Notices of the Royal Astronomical Society*, 176, pp. 249–263. DOI:<https://doi.org/10.1093/mnras/176.2.249>.

Wang, PF and Han, JL and Han, L and Cai, BY and Wang, C and Wang, T and Chen, X and Zhou, DJ and Yu, YZ and Han, J and others., 2020, 'Jiamusi pulsar observations-III. Nulling of 20 pulsars' *Astronomy & Astrophysics*, 644, pp. A73. DOI:<https://doi.org/10.1051/0004-6361/202038867>.

Ziwei Wu, Joris P. W. Verbiest, Robert A. Main, Jean-Mathias Grießmeier, Yulan Liu, Stefan Osłowski, Krishnakumar Mochikallal Ambalappat, Ann-Sofie Bak Nielsen, Jörn Künsemöller, Julian Y. Donner., 2022, 'Pulsar scintillation studies with LOFAR - I. The census' *Astronomy & Astrophysics*, 663, pp. A116. DOI:<https://doi.org/10.1051/0004-6361/202142980>.

Basu, Rahul and Mitra, Dipanjan and Melikidze, George I and Skrzypczak, Anna., 2019, 'Classification of subpulse drifting in pulsars' *Monthly Notices of the Royal Astronomical Society*, 482, pp. 3757–3788. DOI:<https://doi.org/10.1093/mnras/sty2846>.

Johnston, Simon and Mitra, Dipanjan and Keith, Michael J and Oswald, Lucy S and Karastergiou, Aris., 2024, 'The Thousand-Pulsar-Array programme on MeerKAT-XIV. On the high linearly polarized pulsar signals', *Monthly Notices of the Royal Astronomical Society*, 530, pp. 4839–4849. DOI:<https://doi.org/10.1093/mnras/stae1175>.

Lyne, AG and Pritchard, RS and Graham Smith, F., 1993, '23 years of Crab pulsar rotational history', *Monthly Notices of the Royal Astronomical Society*, 265, pp. 1003–1012. DOI:<https://doi.org/10.1093/mnras/265.4.1003>, WEB:<https://www.jb.man.ac.uk/~pulsar/crab.html>

Stappers, B.W., Hessels, J.W.T., Alexov, A., Anderson, K., Coenen, T., Hassall, T., Karastergiou, A., Kondratiev, V.I., Kramer, M., Van Leeuwen, J. and Mol, J.D., 2011, Observing pulsars and fast transients with LOFAR., *Astronomy & astrophysics*, 530, A80. DOI:<https://doi.org/10.1051/0004-6361/201116681>.

van Straten, W., Jameson, A., & Osłowski, S. (2021) 'PSRDADA: Distributed acquisition and data analysis for radio astronomy', *Astrophysics Source Code Library*, ascl-2110. ADS:<https://ui.adsabs.harvard.edu/abs/2021ascl.soft10003V/abstract>.

McKerns, M. M., Strand, L., Sullivan, T., Fang, A., & Aivazis, M. A. (2012), Building a framework for predictive science., *eprint arXiv:1202.1056*, DOI:<https://doi.org/10.48550/arXiv.1202.1056>.

van Straten, W., & Bailes, M. (2011). DSPSR: digital signal processing software for pulsar astronomy., *Publications of the Astronomical Society of Australia*, 28(1), 1-14. DOI:<https://doi.org/10.1071/AS10021>.

Hobbs, G., Manchester, R., Teoh, A., & Hobbs, M. (2004). The ATNF pulsar catalog., *Symposium - International Astronomical Union*, 218, pp 139–140. DOI:<https://doi.org/10.1017/S0074180900180829>.

Lorimer, D. R. (2011). SIGPROC: pulsar signal processing programs., *Astrophysics Source Code Library*, ascl-1107. ADS:<https://ui.adsabs.harvard.edu/abs/2011ascl.soft07016L/abstract>.

Ransom, S. (2011). PRESTO: PulsaR Exploration and Search TOolkit., *Astrophysics source code library*, ascl-1107. ADS:<https://ui.adsabs.harvard.edu/abs/2011ascl.soft07017R/abstract>.

Hotan, A. W., van Straten, W., & Manchester, R. N. (2004). PSRCHIVE and PSRFITS: an open approach to radio pulsar data storage and analysis. *Publications of the Astronomical Society of Australia*, 21(3), 302-309. DOI:<https://doi.org/10.1071/AS04022>.

Harris, Charles R and Millman, K Jarrod and Van Der Walt, Stéfan J and Gommers, Ralf and Virtanen, Pauli and Cournapeau, David and Wieser, Eric

and Taylor, Julian and Berg, Sebastian and Smith, Nathaniel J and others., (2020). Array programming with NumPy. *nature*, 585(7825), pp - 357-362. DOI:<https://doi.org/10.1038/s41586-020-2649-2>.

Lazarus, P and Karuppusamy, R and Graikou, E and Caballero, RN and Champion, DJ and Lee, KJ and Verbiest, JPW and Kramer, M., 2020, 'CoastGuard: Automated timing data reduction pipeline' *Astrophysics Source Code Library*, pp. ascl-2003. ADS:<https://ui.adsabs.harvard.edu/abs/2020ascl.soft03008L/abstract>

Lars Künkel. (2017) 'iterative\_cleaner'. *Github*,. GIT:[https://github.com/larskuenkel/iterative\\_cleaner.git](https://github.com/larskuenkel/iterative_cleaner.git)., Thesis: LOFAR Studies of Interstellar Scintillation., DOC: <https://drive.google.com/file/d/1PPiVaUqosjcTWvA0VUzueJ8YtDfg1G53>

Arul Pandian B. (2026) 'GBD\_DART\_lite'. *Github*,. GIT:[https://github.com/Arul16psp05/GBD\\_DART\\_lite.git](https://github.com/Arul16psp05/GBD_DART_lite.git)., DOI: <https://doi.org/10.5281/zenodo.18184048>

Fitria, Tira Nur. (2021), 'Grammarly as AI-powered English writing assistant: Students' alternative for writing English'. *Metathesis: Journal of English Language, Literature, and Teaching*, 5, pp. 65–78. DOI:<https://doi.org/10.31002/metathesis.v5i1.3519>

Fitria, Tira Nur. (2021), 'QuillBot as an online tool: Students' alternative in paraphrasing and rewriting of English writing'. *Englisia: Journal of Language, Education, and Humanities*, 9, pp. 183–196. DOI:<https://doi.org/10.22373/ej.v9i1.10233>